Materials Advances

ROYAL SOCIETY OF CHEMISTRY

PAPER

View Article Online
View Journal | View Issue

Cite this: *Mater. Adv.*, 2024, 5, 2906

Bimetallic PdPt alloy nanoparticle-decorated track-etched polyethylene terephthalate membranes for efficient H_2 separation†

Nishel Saini, [a] Sonalika Agarwal *[ab] and Kamlendra Awasthi *[a]

To realize hydrogen economy, hydrogen purification is the primary demand, and it can be achieved using membrane technology. Additionally, embedding hydrogen-sensitive materials into the membranes could be a decent approach to reinforce the separation qualities. Bimetallic nanoparticles exhibit novel characteristics due to the synergistic impacts of the two distinct metals. Here, we report the synthesis of PdPt BNPs of around 8 nm size to decorate track-etched polyethylene terephthalate (PET) membranes for boosting hydrogen separation properties. For this purpose, the membranes were dipped into the bimetallic nanoparticle solution at different time gaps of up to 72 hours. The synthesized bimetallic nanoparticles were examined using X-ray diffraction spectroscopy, X-ray photoelectron spectroscopy and transmission electron microscopy techniques, and their uniform distribution over the membranes was confirmed using field emission scanning electron microscopy (FESEM) with EDS mapping. Several approaches have been employed to increase the nanoparticles' adherence to the membrane, including UV functionalization prior to the bimetallic nanoparticle decoration and the usage of polyvinyl-pyrrolidone (PVP) as a binder. The engineered membranes were examined for their permeability towards H_2, N_2 and CO_2 gases. After modifications, the membranes exhibited the highest H_2 permeability of 668 128 barrer and H_2/CO_2 and H_2/N_2 selectivities of 4.18 and 4.01, respectively. In addition, we have attempted to discuss the mechanism of the improvement in the gas separation performance based on the interaction and diffusion of H_2 gas through the membrane. Our findings indicate that the PdPt BNP decoration can effectively enhance the gas separation properties of the membranes.

Received 24th October 2023,
Accepted 5th February 2024

DOI: 10.1039/d3ma00896g

rsc.li/materials-advances

1. Introduction

The growing energy demand in the current scenario and lower fuel availability require shifting to another fuel technology.[1] Hydrogen is a clean, renewable energy carrier that has a high energy density and calorific value. In addition, its only output is water, making it a completely sustainable energy option.[2] However, its purest form is necessary for its use as a fuel. In the pursuit of hydrogen purification, conventional methodologies like cryogenic distillation and the pressure swing method have long held sway; yet, their reliance on substantial resources and heavy equipment has cast a shadow on their sustainability.[3,4]

Membrane technology has the potential to separate a gaseous mixture into its distinct components without heavy set-up and power consumption.[5,6] For this function, a variety of organic and inorganic membranes have been described.[7,8] Out of them, polymer membranes offer a low-cost alternative with superior mechanical and chemical capabilities.[9] Their flexible and lightweight characteristics have made the separation unit portable.[10,11] These polymer membranes can be used in both porous and dense forms as well as they provide the possibility of pre- and post-synthesis modifications.[12] However, despite having several advantages, the overall efficiency of the membranes suffers due to the near-universal trade-off relationship between permeability and selectivity values, *i.e.* if one increases, then the other decreases and *vice versa*.[13]

The aforementioned problem can be tackled by discovering other alternatives to conventional polymer membranes, such as (1) switching to advanced, next-generation polymer materials, (2) utilizing various engineering and modification techniques to enhance the membrane characteristics, *etc.*[14] Engineering polymer membranes to offer uniformity in pore size and pore distribution, attachment of various functional groups and

[a] *Department of Physics, Malaviya National Institute of Technology Jaipur, Rajasthan 302017, India. E-mail: sonalika.spsl@gmail.com, kawasthi.phy@mnit.ac.in*
[b] *Graduate School of Advanced Science and Engineering, Hiroshima University, 1-4-1 Kagamiyama, Higashi-Hiroshima, 739-8527, Japan*

† Electronic supplementary information (ESI) available. See DOI: https://doi.org/10.1039/d3ma00896g

decorating with nanomaterials, has provided the field with a great deal of potential.[15] Various engineering methods such as functionalization and cross-linking,[16] blending with other polymers, and mixing of other metal and non-metal nanoparticles[17] have been reported to improve the separation parameters as well as membrane stability.[18] Although significant progress has been made by the researchers through development of advanced materials and modification processes, but for the better utilization of these membranes in industrial applications, their separation performance must be enhanced along with high yield for large-scale industrial applications.[19] Furthermore, the membranes must be durable and resistant to degradation over time.[20] Extending the lifespan of membranes is crucial for reducing maintenance and replacement costs.[21]

Functionalization is an efficient technique to bestow the membranes with modified and enhanced surface properties.[22] Various physical and chemical approaches have been utilized for the functionalization process,[23] with UV functionalization being the most simple, low-cost, and effective method for surface modification of the membranes.[24,25] Bu *et al.* functionalized poly(arylene ether ketone) membranes under UV irradiation for their usage in electrochemical devices.[26] Kumar *et al.* functionalized track-etched polycarbonate membranes under UV exposure to improve the H_2 gas selectivity over N_2 and CO_2 gases.[27] Hou *et al.* reported enhanced H_2 permeability and H_2/N_2 and H_2/CH_4 selectivity after UV irradiation.[28] Apart from the improvement in gas separation parameters, such UV treatment also increases the active sites on the surface of the polymer membrane through the formation of radicals. Such sites provide a place for the decoration of various nanoparticles to adhere to the membrane surface and pore walls.[29]

Certain metals such as Ni, Pd, and Pt have gained a lot of importance due to their higher affinity towards hydrogen gas.[30,31] The catalytic activity of these metals causes hydrogen molecules to break apart into H-atoms, which subsequently diffuse through the membrane and recombine to create H_2 molecules on the permeate side.[31] However, the high cost, brittle nature, and contamination-related difficulties always limit the widespread application of metal membranes directly.[32] Thus, decorating noble metal nanoparticles on the membrane or mixing them with the polymer matrix is a cost-effective alternative to using dense metal membranes.[33] Strugova *et al.* fabricated $LaNi_5$ and polyethylene-based metal–polymer composite membranes with good H_2/N_2 and H_2/CO_2 selectivity values of 66 and 132, respectively.[34] Also, metal particles in nanomaterial form provide enhanced catalytic performance.[35]

Pd leads to high catalytic dissociation of H_2 molecules on the surface. Better H_2 dissolution in the structure results in higher separation capabilities,[36] consequently enhancing the binding of H_2 gas to the membrane and thereby increasing the separation performance.[37] Kumar *et al.* decorated Pd nanoparticles on UV functionalized track-etched polycarbonate membranes and improved the gas selectivity values from 2.26 to 5.79 and 2.47 to 6.13 towards H_2/N_2 and H_2/CO_2 gases, respectively.[38] In a separate study, they reported functionalized Pd decorated and aligned MWCNTs in the polycarbonate matrix with improved H_2 permeability and H_2/CO_2 selectivity from 2.56 to 7.96.[39] Simon *et al.* reported improved gas separation properties using Pd/polyetherimide nanocomposite asymmetric membranes.[40] Kamakshi *et al.* decorated Pd NPs on carboxylic acid functionalized track-etched PET membranes to enhance H_2/N_2 and H_2/CO_2 selectivity values from 2.04 to 4.27 and 2.01 to 4.28, respectively, along with 2-fold increment in the H_2 permeability.[41] Since both Pd and Pt provide good binding ability toward H_2 gas,[42] the membranes showed improved H_2 separation even at room temperature through the phenomena of physisorption by metal NPs. Patel *et al.* coated a PdPt alloy thin film of 8 nm to 10 nm thickness on a dense polycarbonate substrate using a sputtering technique and increased the H_2 gas permeability value by 17% as compared to the pure PC membrane.[32]

Alloying can alter the electronic band structure and improve the chemical stability of the material. The synergistic effect of alloying the noble metal nanoparticles boosts the chemical activity of the material towards the H_2 molecule. Thus, utilization of the bimetallic nanoparticles can be very effective in enhancing membrane separation parameters. To our knowledge, no research on decorating bimetallic alloy nanoparticles on the surface and pores of polymer membranes has been published. Hence, the novelty of our work is the use of bimetallic alloy nanoparticles. Both Pd and Pt have been extensively studied separately in membrane gas separation, but for the first time their decoration in alloy nanoparticle combination has been carried out to study their impact on the polymer membranes.

In this study, we present the first-ever report on hydrogen separation using PdPt BNP decorated track-etched polymer membranes, where the NP decoration was done using the subsequent dipping process. In order to improve the nanoparticle's adhesion to the membranes, the membranes were subjected to a UV irradiation technique prior to dipping. Furthermore, to ensure appropriate uniform binding of nanoparticles to the polymer membranes, polyvinylpyrrolidone (PVP) is utilized as a binder. PVP is a water-soluble, synthetic polymer made up of linear 1-vinyl-2 pyrrolidone groups. It has abundant binding capacity towards metals, polar compounds, and polar groups due to its strong polarity.[43] Kumar *et al.* from our group have already demonstrated uniform binding of Pd NPs on PC membranes in the presence of PVP. Their findings showcased that these membranes presented maximum selectivity as compared to membranes without PVP due to uniformly attached metal nanoparticles.[27] In this work, our results demonstrate that the membrane surface has been uniformly decorated with PdPt BNPs and that the process is efficient for H_2 separation.

2. Materials and methods

2.1. Materials required

All chemicals were commercially sourced at analytical grade and used without additional purification. Hexadecyltrimethylammonium

chloride (CTAC, $C_{19}H_{42}ClN$, 98%, powder, MW – 320 g mol^{-1}, m.p. – 232–237 °C), hexadecyltrimethylammonium bromide (CTAB, $C_{19}H_{42}BrN$, 99%, powder, MW – 364.45 g mol^{-1}, m.p. 237–243 °C, water soluble, bulk density – 390 kg m^{-3}), palladium chloride ($PdCl_2$, 99%, powder, MW – 177.33 g mol^{-1}, m.p. 678–680 °C, density – 4 g mL^{-1} at 25 °C (lit.)) and dihydrogen hexachloroplatinate hexahydrate ($H_2PtCl_6{\cdot}6H_2O$, ACS reagent, ≥37.50% Pt basis, solid powder/chunks, MW – 517.90 g mol^{-1}) were provided by Sigma Aldrich. Sodium citrate ($C_6H_5Na_3O_7{\cdot}2H_2O$, 98%, white powder, MW – 294.10 g mol^{-1}, m.p. 300 °C, density – 1.008 g mL^{-1} at 20 °C) was purchased from Showa Chemicals. To study the hydrogen separation characteristics, track-etched PET membranes of 30 μm thickness with a uniform pore diameter (0.2 μm) and uniform pore distribution were utilized; these were bought from Sterlitech Corporation, USA. Polyvinylpyrrolidone (PVP, $(C_6H_9NO)_n$, white powder, MW 40 000 g mol^{-1}, density – 1.2 g mL^{-1}) used as a binder was bought from Loba Chemicals, India. All the chemicals were used without any further modification.

2.2. Synthesis of bimetallic PdPt alloy nanoparticles

For the synthesis of PdPt BNPs, firstly, in a 100 mL glass vessel, 80.0 mL of CTAB (15 mM) and 10.0 mL of CTAC (15 mM) deionized (DI) water solutions were combined. The aforementioned solution was then gradually supplemented with 1 mL solutions of H_2PdCl_4 (10 mM) and H_2PtCl_6 (10 mM), which were all stirred at room temperature. Next, an appropriate amount of sodium citrate (100 mM) was added to the resulting solution. After that, the glass vessel was then meticulously sealed, heated for 16 h at 90 °C in the oven, and then allowed to cool naturally. The resultant mixture was centrifuged for 30 minutes at 13 000 rpm to completely isolate the PdPt nanoparticles. After that, distilled water was used to re-disperse the collected PdPt BNPs for future use.

2.3. Membrane modification method

The membranes were initially modified using the UV irradiation method, using a G11T5 lamp at 11 W power having a wavelength of 253.7 nm, lying in the C-region of the UV spectrum. All the membranes were subjected to UV treatment for 48 hours on both sides before being decorated with bimetallic nanoparticles.

During UV irradiation, the membranes were kept at a constant distance from the UV light source. After irradiation, they were immersed in a fixed volume of bimetallic PdPt alloy nanoparticle solution with and without the PVP binder at different pre-decided time differences. For this purpose, a 0.001 g mL^{-1} solution of PVP was prepared. During the membrane modification process, it was ensured that both sides of the membrane received the same treatment to maintain uniformity. Based upon the modification parameters, the details of the samples are listed below in Table 1.

2.4. Characterization techniques

The synthesized PdPt BNPs were characterized using an X-ray photoelectron spectroscopy apparatus, namely the ESCA + Omicron nanotechnology spectrometer, to confirm the formation of PdPt alloy nanoparticles and their binding state. XRD characterization was done using a Panalytical X Pert Pro instrument to confirm the synthesis of bimetallic PdPt alloy nanoparticles. For the morphological analysis, transmission electron microscopy (TEM) was carried out using the instrument Tecnai G2 20 S-TWIN [FEI] at 200 kV. The surface morphology of the membranes was confirmed by using the field emission scanning electron microscopy technique, and the PdPt BNP decoration was confirmed by using FESEM with EDS mapping. The FESEM instrument (Nova Nano FESEM 450) was used with an accelerating voltage of 15 kV. Furthermore, the characteristic bond changes and structural modifications after UV functionalization and nanoparticle decoration were examined using the Fourier transform infrared spectroscopy (FTIR) technique in the range of 400 cm^{-1} to 4000 cm^{-1}, utilizing the Spectrum 2 PerkinElmer set-up. The AIRIX STR 500 Raman spectrophotometer was used to record the Raman spectrum at an excitation laser wavelength of 532 nm, in the range of 400 cm^{-1} to 4000 cm^{-1}.

Table 1 Sample representation depending upon the UV modification and PdPt BNP deposition time

Sample name	UV irradiation time	Bimetallic NP deposition time	Representation
PET 0.2 μm	0 hours	No dipping	Pure PET
PET 0.2 μm	48 hours	No dipping	UV 48 PET
PET 0.2 μm	48 hours	24 hours dipped	24 PdPt
PET 0.2 μm	48 hours	48 hours dipped	48 PdPt
PET 0.2 μm	48 hours	72 hours dipped	72 PdPt
PET 0.2 μm	48 hours	24 hours dipped with PVP	24 PdPt/PVP
PET 0.2 μm	48 hours	48 hours dipped with PVP	48 PdPt/PVP
PET 0.2 μm	48 hours	72 hours dipped with PVP	72 PdPt/PVP

2.5. Gas separation performance

The gas separation properties of the membranes have been studied by using the gas permeability set-up, details of which are given elsewhere.[44] The gas permeability values of the membranes have been calculated by using an equation based on Fick's formula.

$$P = \frac{K \cdot d \cdot s}{\Delta p \cdot t}$$

where K is termed as the cell constant, d is the thickness of the membranes, s is the displacement of a bubble in the bubble meter, Δp is the pressure difference between both sides of the membrane, and t is the time taken. The effective area of the membrane during the gas separation study is 13.19 cm^2. All the gas permeability measurements were taken five times to minimize the chances of error, and also error bars were displayed in the graph to highlight the range of values within which each measurement was obtained. For gas permeability measurements, hydrogen (H_2), carbon dioxide (CO_2) and nitrogen (N_2) gases are used in their purest form (99.999% purity) at room temperature and a pressure of 10 psi.

3. Results and discussion

3.1. Characterization of bimetallic PdPt alloy nanoparticles

Transmission electron microscopy (TEM) and high-resolution transmission electron microscopy (HRTEM) were employed to identify the structural characteristics of the synthesized PdPt BNPs. As depicted in Fig. 1(a and b), the NPs are spherical structures with an average diameter of around 8 ± 2 nm and a maximum number of particles lie in the range from 5 nm to 10 nm (as calculated using the Gaussian fitting; see the inset in Fig. 1(a) for the histogram and particle size distribution). Fig. 1(c) shows the HRTEM analyses of the PdPt BNPs. The obtained value of the interplanar spacing is 0.226 nm, corresponding to the (111) reflections, which can be assigned to Pd or Pt because of the similar values of interplanar spacing in both Pd and Pt. The selected area electron diffraction (SAED) image (Fig. 1(d)) shows the diffraction spot pattern, demonstrating their polycrystalline nature and also a good match with XRD results shown in Fig. 2.

The crystalline structures of the alloy are identified by the X-ray diffraction (XRD) patterns. Fig. 2a displays the XRD patterns of PdPt BNPs in a 2θ range between 35° and 55°. As seen in Fig. 2a, PdPt BNPs exhibited two main diffraction peaks at 39.91° and 46.22° for the (111) and (200) planes, which are intermediate between those of pure Pd (JCPDS 00-005-0681, pink line) and Pt (JCPDS 00-004-0802, blue line). Similar results are also reported in the literature.[45,46] This shifting of peaks indicates the formation of the PdPt alloy nanoparticles. Additionally, the XRD diffraction patterns are also consistent with the SAED patterns of the PdPt BNPs (see Fig. 1(d)).

X-ray photoelectron spectroscopy (XPS) was employed for the detection of surface composition and the chemical status of the bimetallic alloy nanoparticles. The typical XPS spectra of Pd 3d and Pt 4f, obtained from the PdPt networks, are displayed in Fig. 2(b). The electron binding energies of the Pd $3d_{5/2}$ and Pd $3d_{3/2}$ orbitals are shown in a high-resolution survey spectrum in Fig. 2(c). These energies can be further divided into the doublet peaks with binding energies of 334.18 eV and 339.50 eV, which correspond to metallic palladium (Pd^0), and the peaks with binding energies of 334.98 eV and 340.54 eV are assigned to Pd^{II}, indicating that more metallic Pd^0 exists in the PdPt alloy nanoparticles.[47,48] These values show slight variations in binding energy levels, which might be a result of alterations in the chemical environment. The electron binding energies of the Pt $4f_{7/2}$ and Pt $4f_{5/2}$ orbitals are shown in a high-resolution survey spectrum in Fig. 2(d). The Pt 4f peak is deconvoluted into four peaks in Fig. 2(d), indicating various environments. Two binding energy peaks of the Pt $4f_{7/2}$ components can be attributed to the Pt^0 (71.26 eV) and Pt^{II} (72.31 eV) species, respectively, in the deconvoluted spectrum, and the peaks with binding energies of 74.55 and 75.82 eV, which are assigned to Pt^0 and Pt^{II} species of the Pt $4f_{5/2}$ components, can be attributed to the formation of the Pd–Pt alloy.[49,50] The energies of palladium and platinum in bimetallic systems tend to migrate to lower levels, which can be attributed to the charge transfer and electronic disturbances between them. As previously stated, this change in binding energy is due to the alloy formation and influenced by the chemical environment.[51] Additionally, the electrical interaction between Pd and Pt may enhance the nanocomposites' catalytic activity and durability.

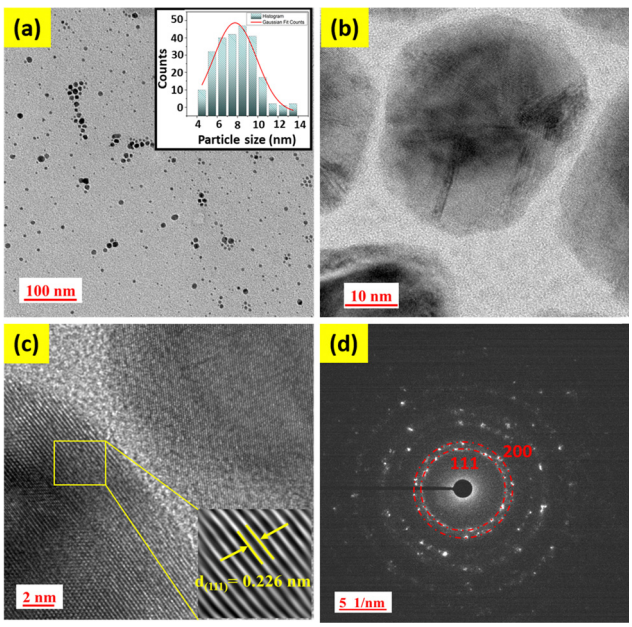

Fig. 1 (a) TEM image with the histogram representing the average particle size in the inset, (b) and (c) HRTEM images, and (d) SAED pattern of PdPt BNPs.

3.2. Fourier transform infrared spectroscopy

Fig. 3 illustrates the FTIR spectrum of the membranes in the range of 400 cm^{-1} to 4000 cm^{-1}. All the membranes contain the bands that represent the characteristic peaks belonging to the core component of PET. The peaks at 506 cm^{-1}, 632 cm^{-1}, and 682 cm^{-1} correspond to –C═O (out-of-plane bending), peaks at 792 cm^{-1} and 846 cm^{-1} correspond to the –C–H bond (in-plane bending), peak at 970 cm^{-1} represents the –COOH band (out-of-plane), and peaks at 1018 cm^{-1}, 1096 cm^{-1} and 1240 cm^{-1} represent the stretching vibrations of the ester bond (C–O)[37,52,53] (see Table 2). Although there is no discernible shift in the spectrum from 400 to 4000 cm^{-1}, certain peaks show variation in the intensity ratio after UV treatment due to the formation of radicals and an increase in the number of certain functionalization groups. For example, the peak at 1716 cm^{-1} represents the stretching vibrations of carboxyl (C═O) groups, and the peak at 724 cm^{-1} represents the stretching vibrations of –C–H (aromatic) groups. After UV functionalization, it can be observed that the carboxyl-to-alkane peak intensity ratio increases from 1.62 to 2.022, confirming that the carbonyl group intensity increases with respect to alkane. Basically, when the PET membranes are subjected to UV irradiation, the polymer deteriorates. This photodegradation is associated with the cleavage of the polymer chain, which results in the increase of hydroxyl and carboxylic acid end groups.

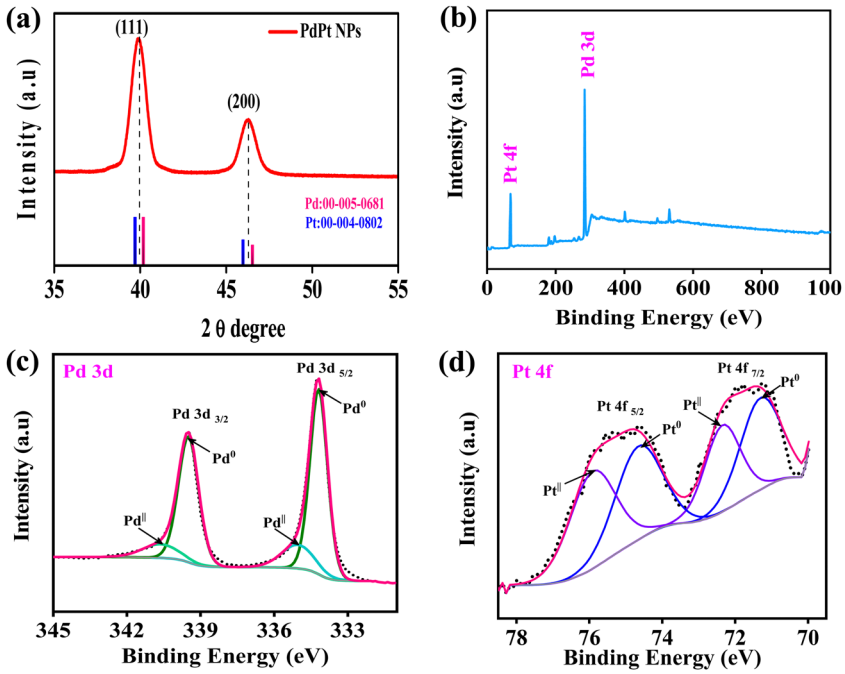

Fig. 2 (a) XRD pattern of PdPt BNPs and XPS spectra survey scan of (b) PdPt BNPs, (c) Pd 3d, and (d) Pt 4f.

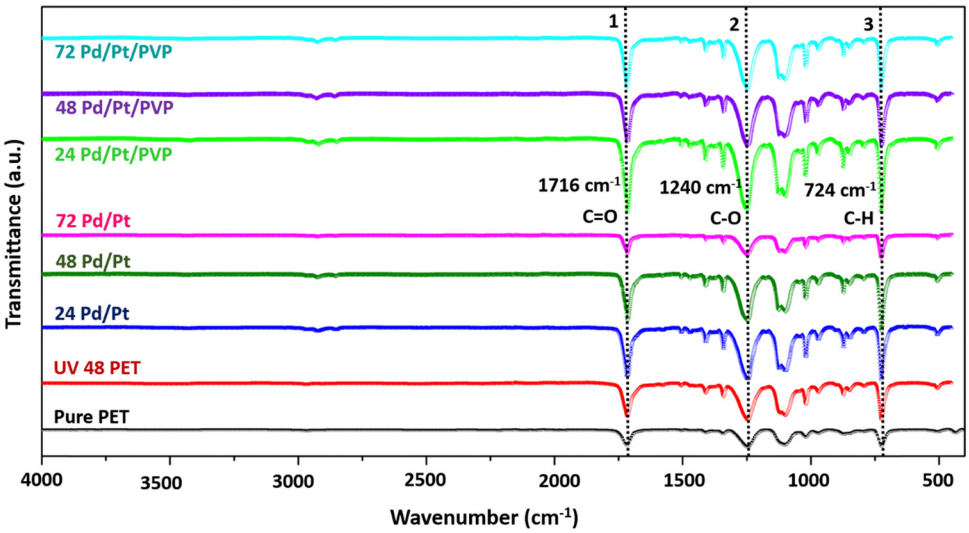

Fig. 3 FTIR spectra of the PdPt BNP modified PET membrane series.

3.3. Raman spectroscopy

Fig. 4(a) presents the Raman spectra of the pure PET membrane and UV treated 72 hour PdPt BNP dipped membrane in the range of 200 cm^{-1} to 2920 cm^{-1} and Fig. 4(b) presents the spectra from 2930 cm^{-1} to 4000 cm^{-1}, respectively. The spectra show the presence of all the fundamental peaks of the PET material, and their corresponding bond assignments in detail are provided in the ESI† (please refer Table S1 in the ESI†).[54] Although there is no remarkable shift in peak positions in the spectra, the intensities of some peaks decrease in the case of modified membranes, indicating the influence of UV treatment.[55] For example, the intensity of the peak at 1612 cm^{-1} represents C=C bond reduction, which may be due to the bond breaking of C=C (unsaturated double bonds). Furthermore, the peak intensities at 1093 cm^{-1} corresponding to C–O–C and at 1727 cm^{-1} corresponding to the stretching C=O group also reduce, while the CH group peak intensity at 1181 cm^{-1} remains unchanged. The reduction in the peak intensity is due to the breakage of the corresponding group or the weakening of that kind of bond. Furthermore, the presence of Pd nanoparticles also results in a lower signal intensity compared with the peak intensity of pure PET

Table 2 Fourier transform infrared peaks of PET membranes and their corresponding bond assignments

Peaks (cm^{-1})	Corresponding bonds
506, 632, 682	–C═O (out-of-plane bending)
724	Stretching vibrations of –C–H (aromatic group)
792, 846	–C–H aromatic group (in-plane bending)
872	Stretching vibration of ═C–H (aromatic group)
970	–COOH (out-of-plane bending)
1018, 1096, 1240	Stretching vibration of C–O (ester bond)
1174	Out-of-plane bending vibration (C–H)
1340	Stretching vibration of –C–H (alkane)
1408, 1504, 1578	Stretching vibration of C═C (aromatic group)
1716	Stretching vibration of the carboxyl bond (C═O)
2968	Stretching vibration of O–H

membranes due to the absorption and scattering from the modified PET membranes. The peaks at 2965 cm^{-1} and 3081 cm^{-1} correspond to methylene groups adjacent to the O atom and aromatic C–H bonds, respectively, as shown in Table S1 (ESI†).[39]

3.4. Field emission scanning electron microscopy

As shown in Fig. 5, the FESEM images were employed for the morphological examination of the membranes. From Fig. 5(a), it is confirmed that the membrane's pore size is nearly equal to 0.2 μm. After the membranes had been treated with UV light, they were dipped into the PdPt BNP solution, and these bimetallic nanoparticles were decorated onto the surface and pore boundaries of the membranes. Bright or yellow points in the FESEM images (shown in Fig. 5(c) and (d)) indicate regions of high roughness, and at these sites, the attachment to the pore boundaries is more likely to occur. The energy-dispersive X-ray spectroscopy (EDS) data of the PET membranes with 48 hours of UV functionalization and 72 hours of PdPt BNP dipping, with and without the PVP binder, respectively, are shown in Fig. 6 and 7. The spectrum confirms the presence and uniform distribution of both Pd and Pt nanoparticles on the membrane surface.

Furthermore, the use of PVP binder has proved to be an effective method to increase the attachment of the bimetallic nanoparticles with the functionalized polymer membrane surface.

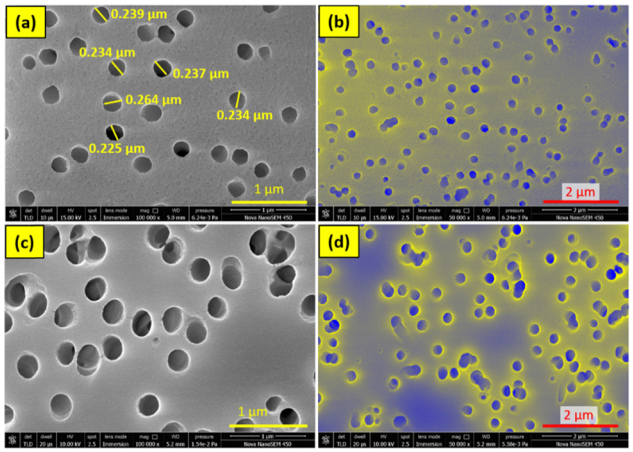

Fig. 5 FESEM images of (a) and (b) pure PET membrane and (c) and (d) 48-hour UV functionalized and 72 hour PdPt BNP dipped PET membrane in the presence of the PVP binder.

3.5. Gas separation performance

The measurements of the membranes' gas permeability were conducted using the H_2, N_2, and CO_2 gases in their purest form (99.999%). Fig. 8 illustrates the separation performance of the membranes, from which we can easily observe that H_2 gas shows the highest permeability value among the other two gases due to its smallest kinetic diameter, better interaction with the modified membrane's surface, high action energy, and greater diffusion within the membrane material. UV functionalization and bimetallic PdPt alloy NPs decoration were further utilized to improve the separation performance resulting in increased H_2 gas permeability and selectivity values. The 72 hour PdPt BNP dipped membrane with PVP showed the highest H_2 gas permeability of 668 128 barrer and H_2/CO_2 and H_2/N_2 selectivity values of 4.18 and 4.01, respectively. The detailed mechanism of the gas separation performance is explained in Section 4. The separation performance was also mapped with the Robeson upper bound, and it was further

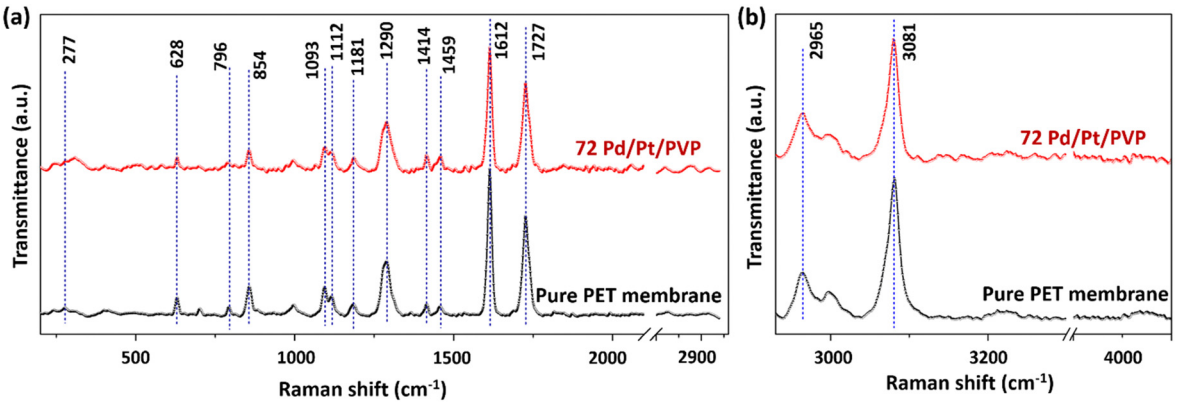

Fig. 4 Raman spectra of the PdPt BNP modified PET membrane series in the ranges of (a) 400 cm^{-1} to 2920 cm^{-1} and (b) 2930 cm^{-1} to 4500 cm^{-1}.

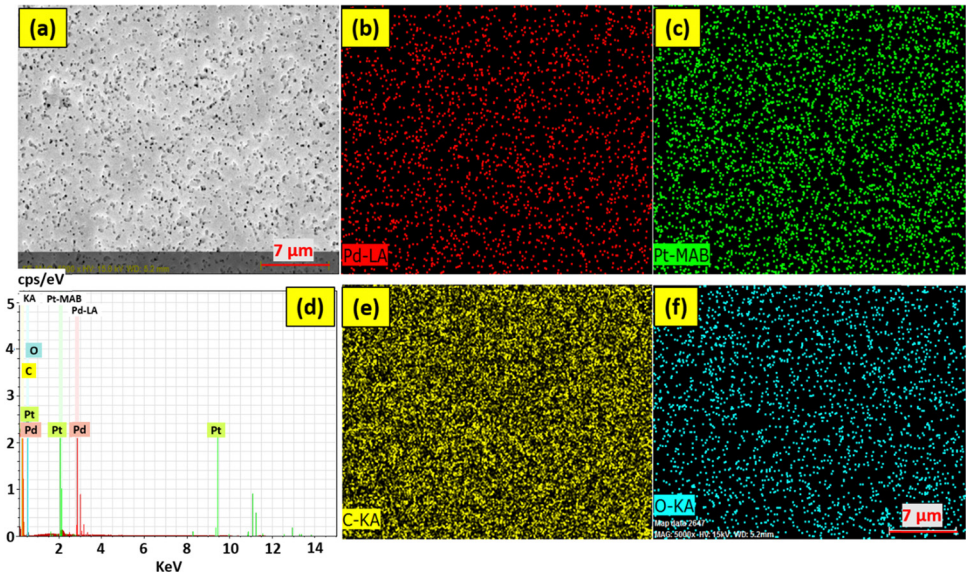

Fig. 6 FESEM with EDS mapping images of 48 hour UV functionalized and 72 hour PdPt BNP dipped PET membrane (in the absence of the PVP binder).

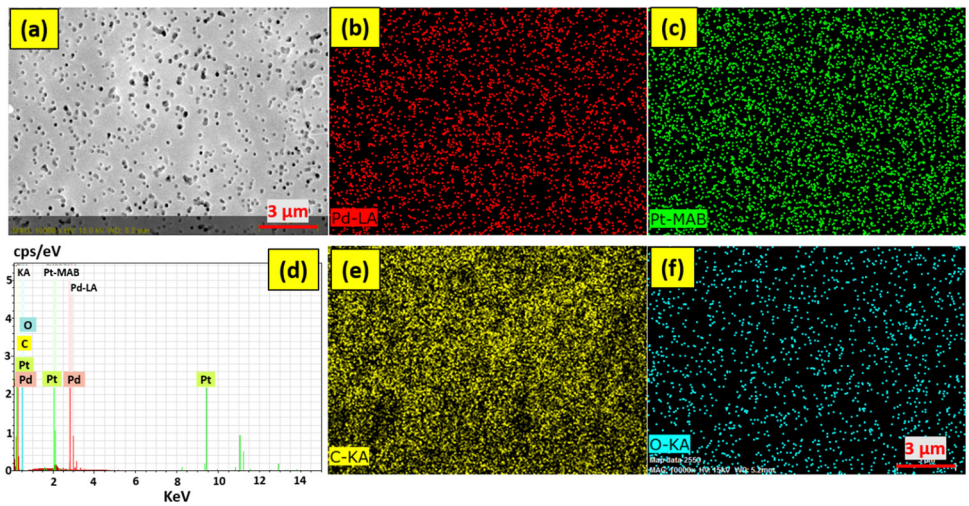

Fig. 7 FESEM with EDS mapping images of 48 hour UV functionalized and 72 hour PdPt BNP dipped PET membrane (in the presence of the PVP binder).

evaluated with the data reported earlier by researchers using differently designed polymer membranes (see Fig. 9 and Table 3). From Fig. 9, it can be concluded that the separation performance has successfully exceeded the Robeson upper bound with a high value of permeability; however, the selectivity still needs to be improved, opening up the potential areas for future research (data table used for the Robeson upper bound comparison obtained from previously reported literature is provided in Table S2 in the ESI†)

4. Gas separation mechanism

The mechanism of gas separation can be explained in such a way that the spherical shape of the H_2 gas molecule as well as certain parameters, such as high activation energy and smaller kinetic diameter, enabled its easy transportation through the pores present in the membranes resulting in high H_2 gas permeability. With UV functionalization, the free radicals on the membrane surface as well as inner pore walls increase, which increases the H_2 gas permeability to an even higher value due to their improved binding with H_2 molecules. The increment in H_2 permeability with UV functionalization has been already reported elsewhere.[28,38] Furthermore, UV functionalization provides the active sites, which help in the attachment of PdPt BNPs with the membrane surface and pore walls. The H_2 gas permeability value again increased when the membranes were decorated with PdPt BNPs due to their higher affinity towards H_2 gas. The PdPt BNPs mostly get adhered to the surface and at the pore walls of the membranes due to the

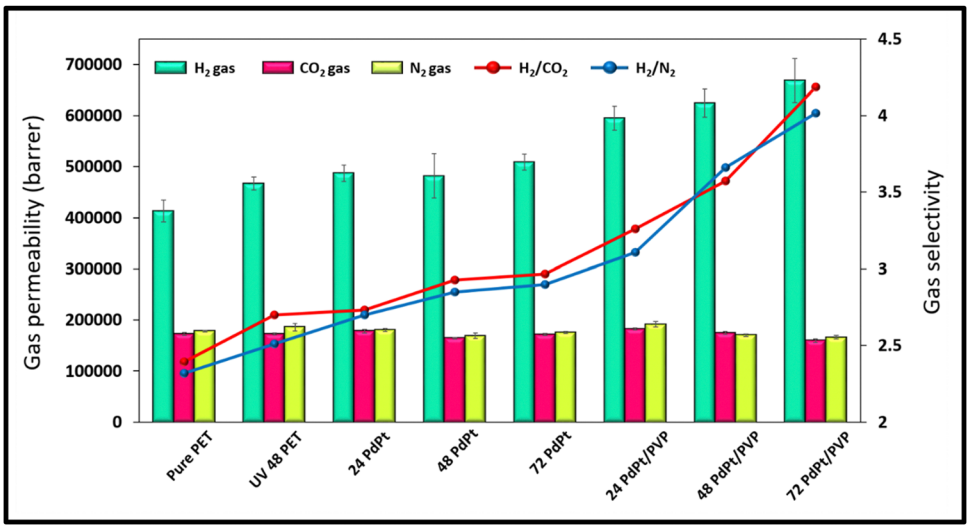

Fig. 8 Gas separation performance of the UV functionalized PdPt BNP dipped PET membrane series.

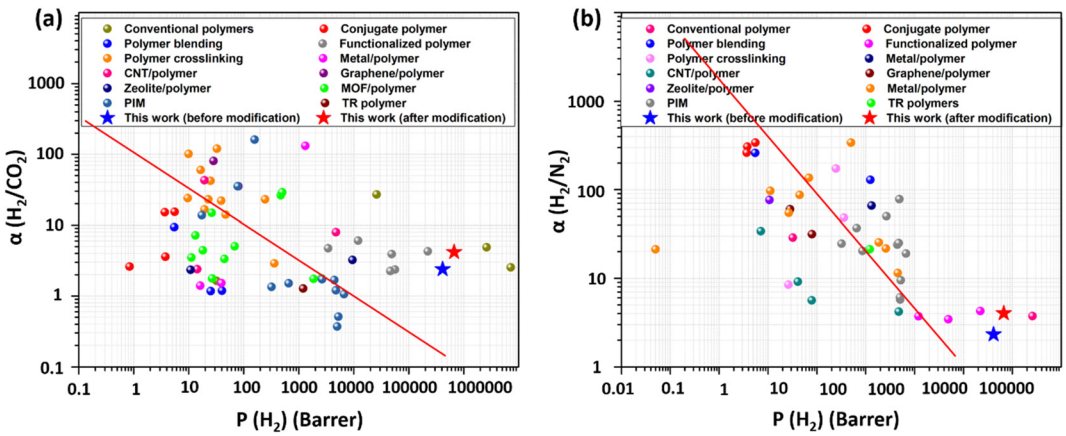

Fig. 9 Comparison of hydrogen separation performance on the Robeson upper bound plot and previously reported studies.

Table 3 Comparison of the experimental results of this work with those of various previously reported studies

Polymers	Fillers	Nature of membrane	Year	H_2 permeability (barrer)	Selectivity values		Ref.
					H_2/N_2	H_2/CO_2	
PC	Ti deposition	Surface coated	2006	3413	4.72	—	56
PC	$Fe_{0.5}Ti_{0.5}$	MMM	2008	—	—	2.5	57
PC	Pd/CNT	MMM	2016	12 211	4.19	7–96	39
PC	Pd–Pt alloy	Surface coated	2018	16.2	—	1.4	32
PC	SiO_2	MMM	2018	39.46	—	1.52	32
Polyethylene	$LaNi_5$	MMM	2018	1320	66	132	34
Track-etched PC	Pd NPs	Surface decorated	2018	49 000	3.92	3.43	27
Polybenzimidazole	Pd	MMM	2021	151.73	—	83.57	58
Track-etched PET	PdPt BNPs	Surface decorated	2023	668 128	4.2	4.01	This work

abundance of functional groups at those sites created after UV functionalization. The gas transfer mechanism is briefly explained in Fig. 10. The H_2 molecules are bound by the bimetallic PdPt alloy NPs in a way that facilitates their movement along the pore walls. However, the molecules of CO_2 and N_2 gases move in a fashion such that there are no appropriate interaction sites available for them to occupy. While in this motion, the molecules are limited in their travel and their high kinetic diameter provides more hindrance to the transportation, making their permeability values remain unaffected even

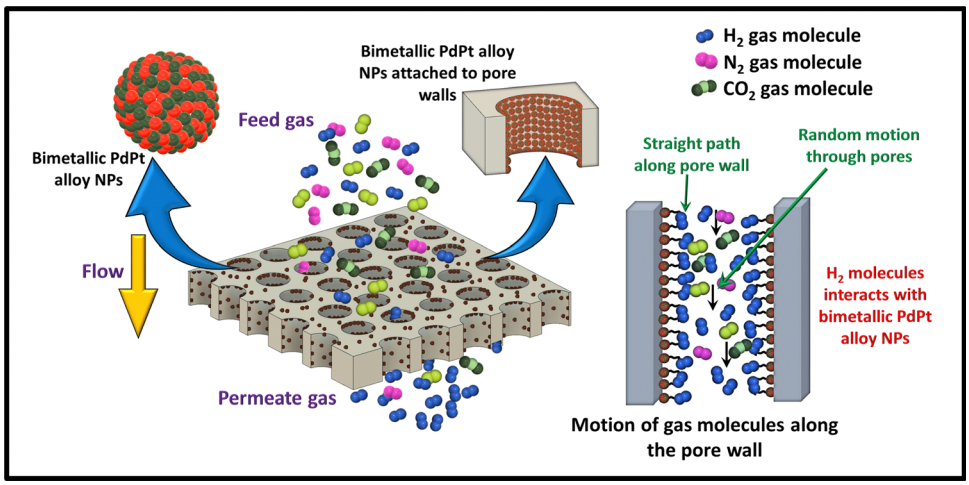

Fig. 10 Schematic representation of the gas separation mechanism of PdPt BNP decorated track-etched polymer membranes.

after the modifications. A similar observation of the gas molecule transportation through nanochannels was also explained elsewhere, where the movement of monoatomic and polyatomic gas molecules through the nanochannels was investigated using the computational tools to study the influence of gas molecule geometry and the gas–pore wall collisions on the gas transportation properties of the membranes.[59] In general, the increased permeability results in enhanced H_2 gas selectivity relative to the other two gases. The presence of the PVP binder further increases the attachment of PdPt BNPs and ensures their uniform distribution, as confirmed by the FESEM EDS mapping images. This is also confirmed here through enhanced gas separation performance. Furthermore, the separation performance of the membranes increases with increasing dipping time in both cases (with and without PVP), and the performance increment is high when the membranes are dipped in the presence of the PVP binder. Both the presence of free radicals and nanoparticles decorated in the pore walls made the environment amenable to H_2 gas. In general, the combination of Knudsen diffusion mechanism and facilitated transport mechanism along the functionalized and bimetallic alloy nanoparticle decorated pores walls leads to enhanced H_2 separation performance of the membranes.

5. Conclusion

Through this work, the effect of PdPt BNP decoration on the hydrogen separation properties of track-etched polymer membranes was studied. PdPt BNPs of particle size around 8 nm were synthesized using the chemical route. These bimetallic nanoparticles were then embellished on track-etched PET membranes modified using UV functionalization. The FTIR spectrum confirms that UV functionalization has successfully generated the functional group sites for the attachment of these bimetallic nanoparticles.

Compared to untreated membranes, the membrane decorated with BNPs for 72 hours in the presence of the PVP binder had a maximum permeability value of 668 128 barrer for H_2 gas, which is an increase of 61%. Moreover, the selectivity between H_2 and CO_2 increases from 2.39 to 4.18 and the selectivity between H_2 and N_2 increases from 2.31 to 4.01, representing a significant increase of 74.89% and 73.59%, respectively.

The track-etched membranes have outperformed previous dense polymer membranes in terms of separation performance, as they showed a greater permeability value. Furthermore, the three main engineering strategies, (i) UV functionalization, (ii) bimetallic PdPt nanoparticle decoration, and (iii) the use of PVP binder, have been proven to be efficient methods to enhance the H_2 separation performance of the membranes.

The current investigation is a pivotal advancement in our quest for the integration of nanoparticles within the membrane matrix. The outcomes presented in this work provide the foundation for the next step—the integration of trimetallic alloy nanoparticles and the use of transition metal atoms. This future step will explore synergistic combinations of noble metal and transition metal atoms, aiming to amplify catalytic properties and bolster the stability of nanoparticles within the membrane. This forward-looking trajectory also includes the substitution of Pt and Pd with alternative transition metal atom nanoparticles, broadening the scope of our research to encompass a more diverse range of materials.

Abbreviations

PdPt BNPs	Bimetallic palladium platinum alloy nanoparticles
PET	Polyethylene terephthalate
FESEM	Field emission scanning electron microscopy
PVP	Polyvinylpyrrolidone
Ni	Nickel
Pd	Palladium
Pt	Platinum
PC	Polycarbonate
CTAC	Hexadecyltrimethylammonium chloride

CTAB	Hexadecyltrimethylammonium bromide
$PdCl_2$	Palladium chloride
Ti	Titanium
$Fe_{0.5}Ti_{0.5}$	Iron titanium alloy
CNT	Carbon nanotube
SiO_2	Silicon dioxide
$LaNi_5$	Lanthanum nickel alloy

Author contributions

Nishel Saini: sample preparation, data collection and analysis, writing original draft; Sonalika Agarwal: sample preparation, data collection and analysis, writing and editing; and Kamlendra Awasthi: conceptualization, supervision and editing. All authors read and approved the final manuscript.

Conflicts of interest

The authors declare that there is no conflict of interest.

Acknowledgements

The author, Nishel Saini, is grateful to the Ministry of Education, India, for providing the fellowship. The authors also acknowledge IUAC, New Delhi (IUAC/UFR/66325) for supporting the work and the Materials Research Center, MNIT Jaipur, for granting the access to characterization facilities.

References

1 H. T. Lu, W. Li, E. S. Miandoab, S. Kanehashi and G. Hu, *Front. Chem. Sci. Eng.*, 2021, **15**, 464.
2 H. Ji, Y. Choi, W. Choi, E. Choi, M. Kim, J. Y. Kim, O. Kwon, Y. Ji and D. W. Kim, *J. Memb. Sci.*, 2023, **683**, 121856.
3 L. Shao, B. T. Low, T. S. Chung and A. R. Greenberg, *J. Memb. Sci.*, 2009, **327**, 18.
4 N. Saini and K. Awasthi, *Sep. Purif. Technol.*, 2022, **282**, 120029.
5 T. Yang and T. S. Chung, *J. Mater. Chem. A*, 2013, **1**, 6081.
6 L. Huang and H. Lin, *Membranes*, 2018, **8**, 100.
7 H. Daglar, I. Erucar and S. Keskin, *Mater. Adv.*, 2021, **2**, 5300.
8 J. E. Lee, C. K. Lim, H. J. Park, H. Song, S. Y. Choi and D. S. Lee, *ACS Appl. Mater. Interfaces*, 2020, **12**, 35688.
9 A. V. Mahenthiran, Z. A. Jawad and B. L. F. Chin, *Environ. Sci. Pollut. Res.*, 2022, 1.
10 S. N. Wijenayake, N. P. Panapitiya, C. N. Nguyen, Y. Huang, K. J. Balkus, I. H. Musselman and J. P. Ferraris, *Sep. Purif. Technol.*, 2014, **135**, 190.
11 J. Widakdo, H. F. M. Austria, T. M. Subrahmanya, E. Suharyadi, W. S. Hung, C. F. Wang, C. C. Hu, K. R. Lee and J. Y. Lai, *J. Mater. Chem. A*, 2022, **10**, 16743.
12 N. Saini, K. Pandey and K. Awasthi, *Mater. Today Chem.*, 2021, **22**, 100558.
13 M. Etxeberria-Benavides, T. Johnson, S. Cao, B. Zornoza, J. Coronas, J. Sanchez-Lainez, A. Sabetghadam, X. Liu, E. Andres-Garcia, F. Kapteijn, J. Gascon and O. David, *Sep. Purif. Technol.*, 2020, **237**, 116347.
14 S. T. Navale, Z. B. Yang, C. Liu, P. J. Cao, V. B. Patil, N. S. Ramgir, R. S. Mane and F. J. Stadler, *Sens. Actuators, B*, 2018, **255**, 1701.
15 S. Zhu, X. Bi, Y. Shi, Y. Shi, Y. Zhang, J. Jin and Z. Wang, *ACS Appl. Nano Mater.*, 2022, **5**, 8997.
16 A. Ebadi Amooghin, H. Sanaeepur, M. Omidkhah and A. Kargari, *J. Mater. Chem. A*, 2018, **6**, 1751.
17 C. Liang, L. Huang, X. Lv, J. Wang, L. Li, X. Li and Z. Wei, *ACS Appl. Nano Mater.*, 2023, **6**, 2995.
18 G. Dianat, N. Movsesian and M. Gupta, *ACS Appl. Polym. Mater.*, 2020, **2**, 98.
19 R. S. Murali, A. Jha, N. Aarti, S. Divekar and S. Dasgupta, *Mater. Adv.*, 2023, **4**, 4843.
20 P. Choudhary, N. Saini, M. H. Yoon, K. Awasthi and K. Pandey, *Environ. Sci. Pollut. Res.*, 2023, **1**, 1.
21 J. Chapman, N. Garapati, V. A. Glezakou, Y. Duan, J. Hu and C. Z. Dinu, *Mater. Adv.*, 2021, **2**, 5922.
22 S. Yi, X. Ma, I. Pinnau and W. J. Koros, *J. Mater. Chem. A*, 2015, **3**, 22794.
23 B. Ghalei, Y. Kinoshita, K. Wakimoto, K. Sakurai, S. Mathew, Y. Yue, H. Kusuda, H. Imahori and E. Sivaniah, *J. Mater. Chem. A*, 2017, **5**, 4686.
24 S. L. Gao, R. Häler, E. Mäder, T. Bahners, K. Opwis and E. Schollmeyer, *Appl. Phys. B*, 2005, **81**, 681.
25 P. Falkenstein, D. Gräsing, P. Bielytskyi, W. Zimmermann, J. Matysik, R. Wei and C. Song, *Front. Microbiol.*, 2020, **11**, 689.
26 F. Bu, C. Zhao Baolong Wang, N. Zhang, H. Lu, Z. Cai, Y. Zhanga and H. Na, *RSC Adv.*, 2015, **5**, 57067.
27 R. Kumar, Kamakshi, S. Shisodia, M. Kumar and K. Awasthi, *Int. J. Hydrogen Energy*, 2018, **43**, 21690.
28 R. Hou, S. J. D. Smith, K. Konstas, C. M. Doherty, C. D. Easton, J. Park, H. Yoon, H. Wang, B. D. Freeman and M. R. Hill, *J. Mater. Chem. A*, 2022, **10**, 10107.
29 I. Hossain, D. Kim, A. Z. Al Munsur, J. M. Roh, H. B. Park and T. H. Kim, *ACS Appl. Mater. Interfaces*, 2020, **12**, 27286.
30 S. P. Cardoso, I. S. Azenha, Z. Lin, I. Portugal, A. E. Rodrigues and C. M. Silva, *Sep. Purif. Rev.*, 2018, **47**, 229.
31 J. J. Conde, M. Maroño and J. M. Sánchez-Hervás, *Sep. Purif. Rev.*, 2017, **46**, 152.
32 A. K. Patel and N. K. Acharya, *Int. J. Hydrogen Energy*, 2018, **43**, 21675.
33 V. Zadorozhnyy, V. Soprunyuk, S. Klyamkin, M. Zadorozhnyy, E. Berdonosova, I. Savvotin, A. Stepashkin, A. Korol, A. Kvaratskheliya, D. Semenov, J. Eckert and S. D. Kaloshkin, *J. Alloys Compd.*, 2021, **866**, 159014.
34 D. V. Strugova, M. Y. Zadorozhnyy, E. A. Berdonosova, M. Y. Yablokova, P. A. Konik, M. V. Zheleznyi, D. V. Semenov, G. S. Milovzorov, M. Padaki, S. D. Kaloshkin, V. Y. Zadorozhnyy and S. N. Klyamkin, *Int. J. Hydrogen Energy*, 2018, **43**, 12146.

35 A. E. Lewis, D. C. Kershner, S. N. Paglieri, M. J. Slepicka and J. D. Way, *J. Memb. Sci.*, 2013, **437**, 257.
36 C. Li, H. Xu, C. Bao and S. Hou, *ACS Appl. Nano Mater.*, 2019, **2**, 3377.
37 Kamakshi, R. Kumar, V. K. Saraswat, M. Kumar and K. Awasthi, *Int. J. Hydrogen Energy*, 2020, **45**, 18676.
38 R. Kumar, Kamakshi, M. Kumar and K. Awasthi, *Environ. Sci. Pollut. Res.*, 2020, 1–10.
39 R. Kumar, Kamakshi, M. Kumar and K. Awasthi, *Int. J. Hydrogen Energy*, 2016, **41**, 23057.
40 S. Simon and E. Espuche, *Sep. Purif. Technol.*, 2014, **129**, 41.
41 Kamakshi, R. Kumar, V. K. Saraswat, M. Kumar and K. Awasthi, *Pure Appl. Chem.*, 2018, 1063–1071.
42 S. Agarwal, M. J. Ahemad, S. Kumar, D. Van Dung, P. Rai, M. Kumar, K. Awasthi and Y. T. Yu, *J. Alloys Compd.*, 2022, **900**, 163545.
43 T. K. Sinha, J. H. Lim, H. R. Chothe, J. G. Kim, T. Nam, T. Lee and J. S. Oh, *J. Appl. Polym. Sci.*, 2022, **139**, 52396.
44 N. Pal, N. Saini, M. Agarwal and K. Awasthi, *Int. J. Hydrogen Energy*, 2022, **47**(99), 41820–41832.
45 A. Aygun, F. Gulbagca, E. E. Altuner, M. Bekmezci, T. Gur, H. Karimi-Maleh, F. Karimi, Y. Vasseghian and F. Sen, *Int. J. Hydrogen Energy*, 2023, **48**, 6666.
46 C. A. Rodríguez-Proenza, J. P. Palomares-Báez, M. A. Chávez-Rojo, A. F. García-Ruiz, C. L. Azanza-Ricardo, A. Santoveña-Uribe, G. Luna-Bárcenas, J. L. Rodríguez-López and R. Esparza, *Mater*, 2018, **11**, 1882.
47 G. Yang, J. Yang, L. Li, P. Lv, Y. Sun, Z. Yuan and J. Yang, *ChemistrySelect*, 2018, **3**, 10768.
48 Y. Liu, S. Liu, Z. Che, S. Zhao, X. Sheng, M. Han and J. Bao, *J. Mater. Chem. A*, 2016, **4**, 16690.
49 R. Sarkar, L. S. Graves, J. R. Taylor and I. U. Arachchige, *ACS Appl. Mater. Interfaces*, 2023, **15**, 50981.
50 J. X. Tang, Q. S. Chen, L. X. You, H. G. Liao, S. G. Sun, S. G. Zhou, Z. N. Xu, Y. M. Chen and G. C. Guo, *J. Mater. Chem. A*, 2018, **6**, 2327.
51 R. K. Pramadewandaru, Y. W. Lee and J. W. Hong, *RSC Adv.*, 2023, **13**, 27046.
52 R. Kumar, Kamakshi, M. Kumar and K. Awasthi, *Int. J. Hydrogen Energy*, 2017, **42**, 15203.
53 Z. Chen, J. N. Hay and M. J. Jenkins, *Eur. Polym. J.*, 2012, **48**, 1586.
54 Z. Zuo, K. Zhu, C. Gu, Y. Wen, G. Cui and J. Qu, *Appl. Surf. Sci.*, 2016, **379**, 66.
55 E. Rebollar, S. Pérez, M. Hernández, C. Domingo, M. Martín, T. A. Ezquerra, J. P. García-Ruiz and M. Castillejo, *Phys. Chem. Chem. Phys.*, 2014, **16**, 17551.
56 N. K. Acharya, V. Kulshrestha, K. Awasthi, R. Kumar, A. K. Jain, M. Singh, D. K. Avasthi and Y. K. Vijay, *Vacuum*, 2006, **81**, 389.
57 Y. K. Vijay, *Int. J. Hydrogen Energy*, 2008, **33**, 340.
58 H. S. M. Suhaimi, C. P. Leo and A. L. Ahmad, *Int. J. Energy Res.*, 2021, **45**, 15171.
59 J. H. Qian, H. A. Wu and F. C. Wang, *Appl. Surf. Sci.*, 2023, **611**, 155613.